A Combined Experimental/Numerical Study of Unsteady Phenomena in a Laminar Separation Bubble

O. Marxen, M. Lang, U. Rist, S. Wagner

Institut für Aerodynamik und Gasdynamik (IAG), Universität Stuttgart

Pfaffenwaldring 21, 70550 Stuttgart, Germany, email: olaf.marxen@iag.uni-stuttgart.de

Abstract. A laminar boundary layer separates in a region of adverse pressure gradient on a flat plate and undergoes transition. Finally the turbulent boundary layer reattaches, forming a laminar separation bubble (LSB). Laminar-turbulent transition within such a LSB is investigated by means of Laser-Doppler-Anemometry (LDA), Particle Image Velocimetry (PIV), and direct numerical simulation (DNS). The transition mechanism occurring in the flow-field under consideration is discussed in detail. Observations for the development of small disturbances are compared to predictions from viscous linear instability theory (Tollmien-Schlichting instability). Non-linear development of these disturbances and their role in final breakdown to turbulence is analysed.

Keywords: transition, instability, separation, DNS, LDA, PIV

1 Introduction

Transition to turbulence in a laminar separation bubble in low free-stream turbulence-level environments is caused by strong amplification of small disturbances. Since velocity profiles in the separated region possess an inflection point, amplification of these two-dimensional disturbances is often attributed to an inviscid mechanism as in free shear-layers (Kelvin-Helmholtz instability). Considerable discussion is still ongoing as to the origin of three-dimensionality and the impact of three-dimensional disturbances on the transition process.

Recent investigations of laminar separation include an experimental study of a LSB excited by an impulsive point-source disturbance [12]. There, the exponential growth of a travelling wave-packet was attributed to a linear behaviour, but no attempt to compare results to linear theories was made. Transition in a LSB employing DNS was examined in [1] with controlled disturbance forcing. In addition, inflectional velocity profiles fitted to the DNS results were theoretically studied to determine parameters for the onset of absolute instability, but without direct comparison to DNS results. In [10] it is suspected that Kelvin-Helmholtz instability is involved in their DNS of the unforced breakdown process in a LSB. The occurrence of a region dominated by Kelvin-Helmholtz

instability is discussed in detail in [13], concluding that the separation bubble is likely to become inviscidly unstable via the Kelvin-Helmholtz mechanism. In [8] it was shown that viscous linear stability theory can be reliably applied for quantitative prediction of two- and three-dimensional disturbances using base-flow profiles from DNS.

Concerning the onset of three-dimensionality, [8] concluded that secondary amplification according to Floquet theory, is unlikely to be observed in LSB's. Instead, they propose breakdown of weakly-oblique travelling waves as the probably fastest route to turbulence in certain types of separation bubbles. Recently, a mechanism of absolute secondary instability of three-dimensional disturbances in separation bubbles with fairly strong pressure gradients and/or high Reynolds number Re_{δ_1} at separation was discovered ([6]).

Despite all these efforts, no detailed quantitative comparison of numerical results and experimental data obtained in a LSB has been made up to now, in particular for unsteady phenomena. In the present work it will be shown that by mutual comparison of results from direct simulations and measurements, supplemented by predictions from linear theory, mechanisms leading to the breakdown to turbulence in existing experimental facilities can be identified in a way that is not possible when applying only one of these methods.

2 Investigation Methods and General Properties of the Flow Field

In this section, experimental and numerical methods applied to the investigation of the flow field containing a LSB are described. This includes the methods of generation of the unsteady LSB as well as observation strategies for the most important flow variables of the ongoing physical processes. General properties of the LSB under consideration are compared for the experimental and numerical case to be used as a base flow for subsequent theoretical stability investigations.

Transition in the experimental case is triggered by a combination of two- and three-dimensional steady and unsteady disturbances. In the DNS, the disturbed modes are chosen in a way that the experiment is accurately modelled as will be shown later. DNS can be applied as a tool to extract the effect of certain disturbances on transition location and general properties of the LSB.

2.1 Experimental Set-Up

The laminar water tunnel at the IAG was especially designed to study transition in a Blasius boundary-layer and in a separation bubble [11]. A flat plate

with an elliptical leading edge is mounted in the free stream of the test section. Because of the large scales and low frequencies in water, this facility is very suitable for flow visualisation and measurements with high resolution in space and time. A streamwise pressure gradient is imposed on the flat-plate boundary-layer by a displacement body. In the region of adverse pressure gradient ($x > 0\ mm$), a pressure induced laminar separation bubble is generated (Fig. 1). To prevent separation and transition on the displacement body itself, the boundary layer is sucked off.

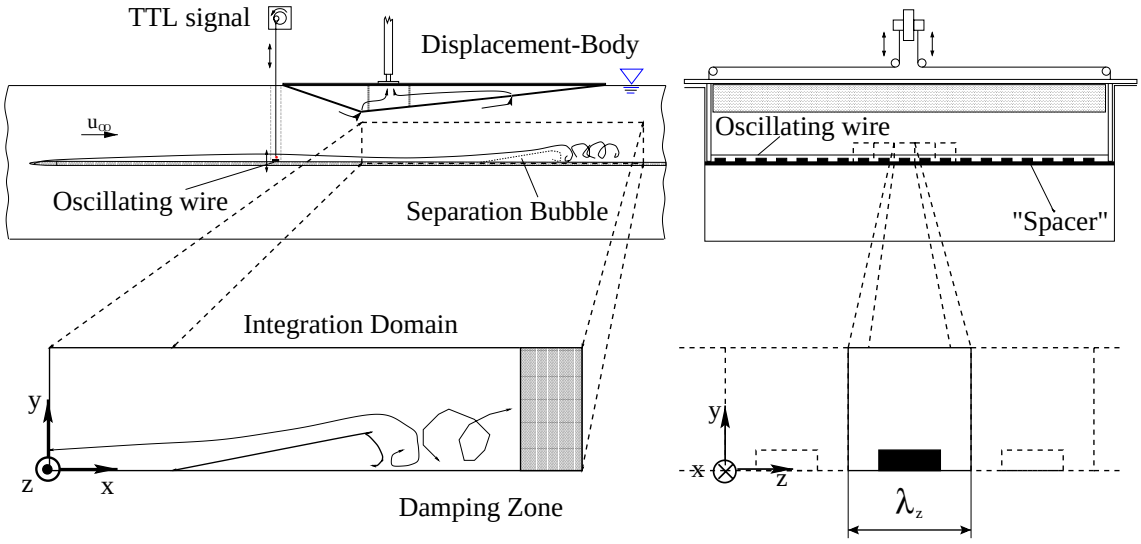

Fig. 1: Experimental set-up and numerical integration domain

The experiment is performed under controlled conditions. A small amplitude 2-D harmonic wave is excited upstream of the displacement body by an oscillating wire. Additionally, 3-D disturbances are imposed by placing thin metal plates (spacers) regularly underneath the wire [3, 4]. All measurements are carried out phase-locked with respect to a reference signal from the disturbance source. The fundamental frequency ($f_0 = 1.1Hz$) corresponds to the frequency which is most amplified according to linear stability theory. The spanwise wavelength of the 3-D disturbance input is set to $\lambda_z = 58\ mm$, so that regularly appearing vortex structures can be seen in the transition region (Fig. 2).

The applied 2-D LDA (Dantec) measures the velocity components $U(t)$ in mean flow direction and the vertical component perpendicular to the flat plate $V(t)$. The PIV system was composed in cooperation with the Deutsche Forschungszentrum für Luft- und Raumfahrt (DLR). It consists of a double pulsed Nd:YAG laser ($150\ mJ/pulse$), a high resolution CCD-camera (PCO SensiCam, $1280\ px \times 1024\ px$) and an external sequencer. The good optical access to the test section of the laminar water-tunnel allows PIV measurements

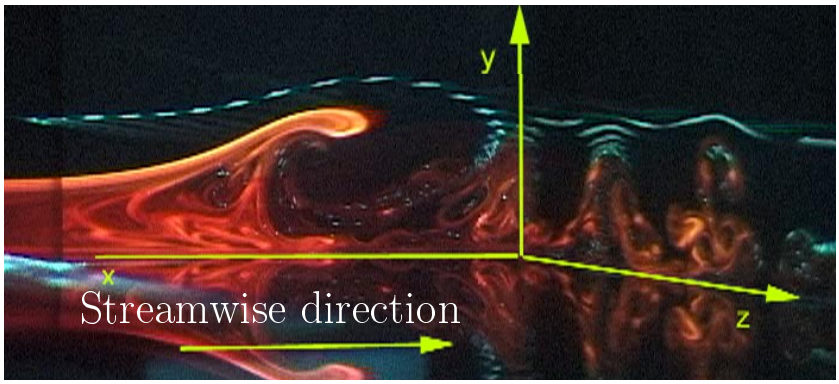

Fig. 2: Flow visualization in the transition region. Two simultaneous Laser light sheets in xy-plane and yz-plane ($x = 330\ mm$), respectively.

to be carried out in all cartesian planes. Thus, phase-locked PIV measurements can be performed including the spanwise velocity component W, which is not accessible with the 2-component LDA. This gives an important insight into appearing vortex structures during the rapid 3D-development of the transitional boundary layer.

In contrast to hot-film anemometry, both applied non-intrusive measurement techniques provide the possibility to identify velocities with their magnitude and direction. In the transition region with its strong bidirectional velocity fluctuations, this is an important benefit. Thus, the dividing streamline can be determined directly from the measured velocity profiles.

LDA measurements were performed in streamwise and spanwise direction. The resolution in span was 16 points per λ_z and the record length of all measured points was about 30 wire cycles.

For an exact determination of the amplitudes and phases of the oscillations in the flow a phase-averaging technique with respect to the oscillating wire is used [4, 5]. A double Fourier transform in time and spanwise direction of phase-averaged LDA data sets yield the amplitudes $a_{h,k}$ and phases $\Phi_{h,k}$ of the measured disturbance waves. The indices h and k denote wave-number coefficients in time and spanwise direction, respectively. Below, the notation (h, k) will be used to specify the modes.

2.2 Numerical Method for DNS and Calculation Parameters

Spatial direct numerical simulation (DNS) of the three-dimensional incompressible Navier-Stokes equations is used to compute the pressure induced LSB described in the previous section. Fourth-order accurate finite differences are used for downstream and wall-normal discretization, while a spectral ansatz is

applied in spanwise direction. A fourth-order Runge-Kutta scheme is used for time integration. Upstream of the outflow boundary a buffer domain smoothly returns the flow to a steady laminar state. The applied numerical method was already described in detail in [7]. A small-amplitude two-dimensional time-harmonic wave with period $T_{2D} = 1/f_0 \approx 0.9s$ is forced upstream of the LSB via blowing/suction at the wall. Additional steady spanwise-harmonic disturbances are excited by wall blowing/suction.

Physical parameters of the flow are chosen to match the experimental setup introduced before. Numerical parameters are shown in table 1 (case LSB3D). The inflow is placed at the position of the narrowest cross section, resulting in a computational domain as drawn in Fig. 1. Its spanwise extent is a single spacer wavelength. The resolution was confirmed to be sufficient by a calculation with increased number of grid points (approximately by a factor of 1.5 in each direction) yielding the same results for the quantities under consideration in this paper. The discretization in x results in approximately 120 grid points per streamwise wavelength of the fundamental wave.

A streamwise pressure gradient is imposed by prescribing a potential velocity distribution for the streamwise velocity $u_{potential}$ at a constant distance y from the wall (Fig. 3, dashed line), while the displacement effect of the boundary layer is captured by a boundary-layer interaction-model [7].

The velocity profile at the inflow boundary ($x = 0mm$) of case LSB3D was obtained from a preceding two-dimensional DNS (case ACC2D) of a strongly accelerated boundary layer, starting from a Falkner-Skan solution ($Re_{\delta_1} = 810, H_{12} = 2.53$) at $x = -400mm$. The favourable pressure gradient was chosen to match the experimental values beyond the narrowest section (Fig. 3), however without strong deceleration. With this precursor calculation, the experimental inflow profile for subsequent case LSB3D could be retrieved (Fig. 4).

The potential velocity distribution $u_{potential}$ used in case LSB3D is chosen according to measurements where separation was suppressed by artificially causing transition prior to the laminar separation point (Fig. 3, open symbols). The mean edge-velocity distribution u_e emerging from the interaction-model almost matches the experimental measurements with separation bubble (Fig. 3, filled symbols). Since this velocity condition at the upper boundary is not

Case	Type	Grid pts.	$\Delta t/T_{2D}$	$x_L[mm]$	$y_L[mm]$	$z_L[mm] = \lambda_z$
ACC2D	2D	3330×185	600	1700	50	-
LSB3D	3D	$1778 \times 185 \times 27$	600	800	50	58

Tab. 1: Computational parameters and box size.

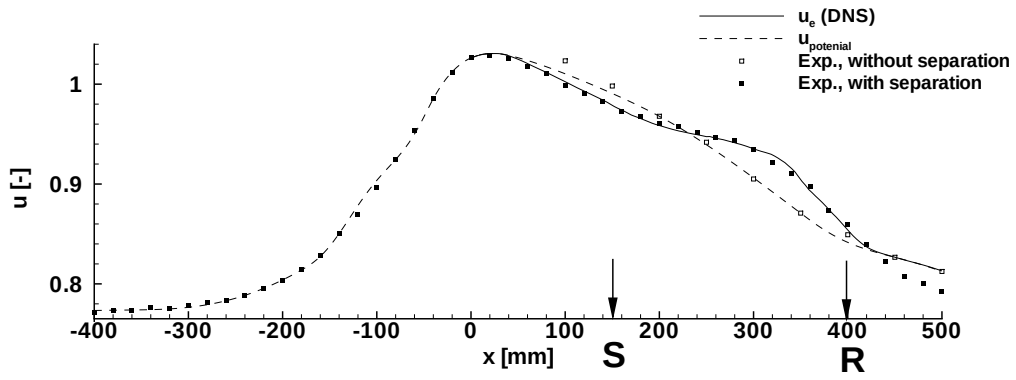

Fig. 3: Streamwise mean velocity at $y = 50\ mm$. DNS results u_e for case LSB3D, potential velocity $u_{potenial}$ prescribed in DNS cases ACC2D and LSB3D; LDA measurements with and without separation.

fixed in advance, it should already be considered a result of the DNS. Good agreement of DNS data with experiments therefore gives a first evidence of the comparability of the separation bubble observed in the experiment and in the DNS. Furthermore, it should be emphasised that the actual velocity prescribed at the upper boundary is highly unsteady from $x \approx 320\ mm$ onwards.

2.3 General Properties of the Laminar Separation Bubble

Computing boundary-layer properties in strongly accelerated/decelerated flow-fields cannot be done in a straightforward way because of considerable velocity changes in the potential flow-region. Following [10], the displacement thickness δ_1 is computed using a pseudo-velocity $\breve{u}$ based on the spanwise vorticity ω_z:

$$\breve{u}(x,y) = \int_0^y \omega_z(x,s)ds, \quad \delta_1(x) = \int_0^y \left(1 - \frac{\breve{u}(x,y)}{\breve{u}_{Max}(x)}\right) ds.$$

In the experimental case, the streamwise resolution is too coarse to calculate the vorticity. However, it can be shown that the potential streamwise velocity close to the plate is proportional to y^2. Thus, the pseudo-velocity $\breve{u}$ is calculated according to:

$$\breve{u}_{Exp}(0,y) = u(0,y) - c \cdot y^2,$$

where the coefficient c is determined by a best fit to the measured data. As can be seen from Fig. 4, the pseudo-velocities $\breve{u}_{pseudo}$ in the numerical and experimental case perfectly agree with each other. Furthermore, the difference to the true velocity is clearly visible. The maximum pseudo-velocity $\breve{u}_{Max} =$

	$Re_{\delta_1}^{x=0}$	$H_{12}^{x=0}$	$H_{32}^{x=0}$	$Re_{\delta_1}^{x=x_s}$	$Re_{\delta_2}^{x=x_s}$	$x_s[mm]$
DNS	428	1.89	1.69	905	282	150
EXP	485	1.85	1.70	950	320	150

Tab. 2: Mean boundary-layer properties.

$\breve{u}(x, y_{max})$ in the smallest cross section ($x = 0\ mm$) serves as a reference velocity to normalize velocities.

In Tab. 2, a comparison of some boundary-layer parameters at inflow and at separation is given, while Fig. 4 (right) compares mean streamwise velocity profiles. Good agreement between DNS results and measurements reveals that a separation bubble of approximately the same size and with the same amount of reverse flow is formed. The last x position is close to the transition location.

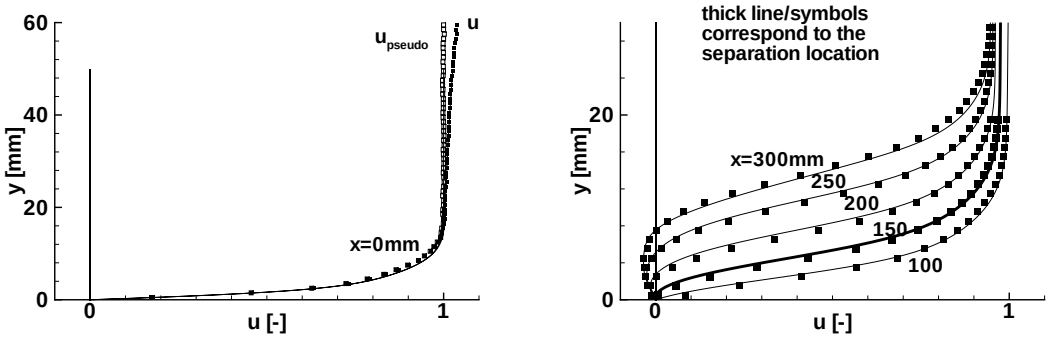

Fig. 4: Streamwise mean velocity profiles (averaged in time and span) at several streamwise positions up to the transition location (DNS: lines, Exp.: symbols).

3 Theoretical Analysis of Stability Properties of the Laminar Separation Bubble with Respect to Small Disturbances

Linear stability theory (LST) is employed to describe the behaviour of small disturbances. Solving the Orr-Sommerfeld equation for the spatial case gives the complex eigenvalue α, where α_r is the streamwise wave-number and α_i the streamwise amplification-rate, and $\omega_r = 2\pi/f$ is the prescribed circular frequency with the temporal amplification-rate ω_i set to 0. The real spanwise wave-number is denoted as $\gamma = 2\pi/\lambda_z$. Resulting viscous instability waves are known as Tollmien-Schlichting (TS) waves.

The investigations in this section are carried out a posteriori, using the time-averaged flow-field just described as the underlying base flow. Since up to a position close to roll-up of the shear-layer ($x = 320\ mm$) the disturbances remain fairly small ($\leq 10\%$), time-averaging is justified. However, it should be stated that the LSB is quite sensitive to small disturbances even in its mean properties ([2]). This sensitivity is not subject of the present paper.

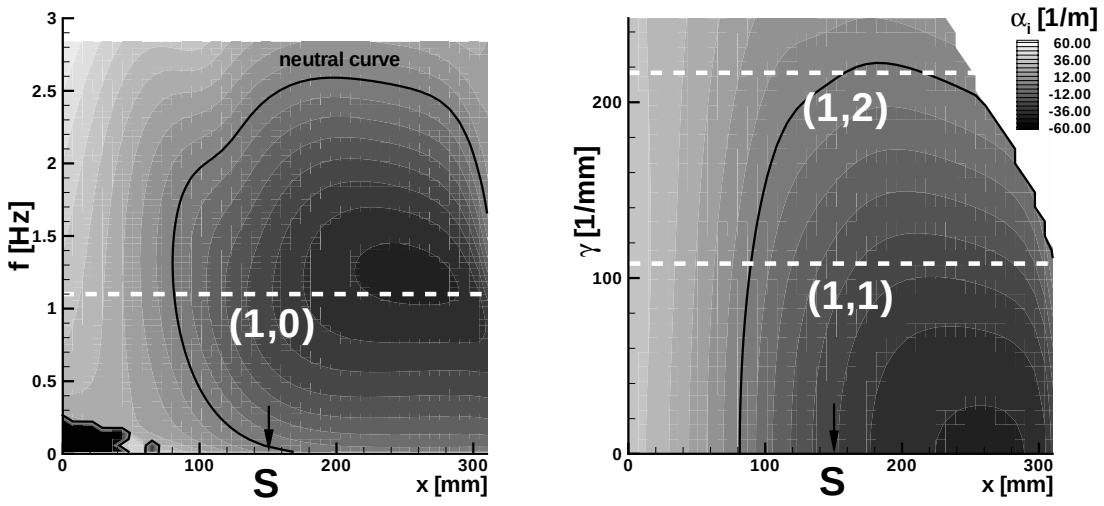

Fig. 5: Stability diagram for the spatial case ($\omega_i = 0$) calculated from the Orr-Sommerfeld equation for $\gamma = 0$ (left) and $\omega_r = 5.71\ s$ (right).

In Fig. 5 stability diagrams are shown. It can be seen that amplification starts prior to separation ($x_s \approx 150\ mm$) and that a wide range of amplified frequencies exists within the separation bubble. The frequency of the harmonic wave forced in DNS and experiment (dashed line in left part of Fig. 5) corresponds to the overall most amplified frequency. This mode (1,0) will later be denoted as TS-mode. Furthermore, it can be seen that two-dimensional disturbances are stronger amplified than oblique waves (right part of Fig. 5).

4 Comparison of Results from DNS, Experiment and LST

Since the LSB is of highly unsteady character as emphasised before, it appears inevitable to consider fully time- and space-resolved disturbance quantities before claiming that the same physics are captured in the numerical and experimental investigations.

The first section of the LSB is dominated by a primary convective instability of the two-dimensional TS-wave (see [6]). Therefore, the development of the 2-D TS wave appears to be very important and is examined in detail. Fig. 6 shows the amplification curve for the streamwise velocity. It can be seen that the TS wave $(1,0)$ is strongly amplified in the region of adverse pressure gradient. Experimental and numerical results perfectly match from $x = 230\ mm$ onwards even shortly beyond saturation of the disturbance amplitude. Good agreement with linear stability theory (LST) confirms the primary convective

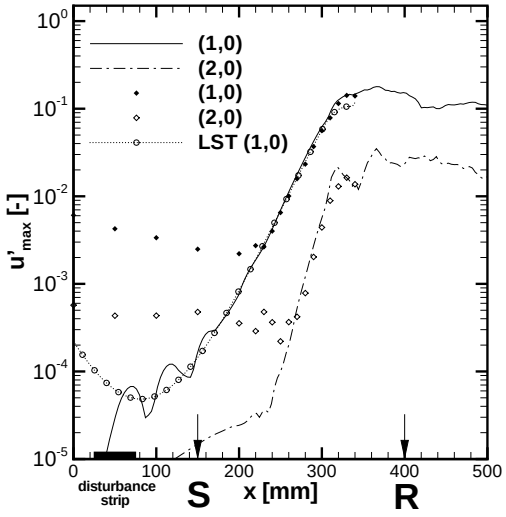

Fig. 6: Amplification of the max. velocity fluctuation u'_{max}. Results from DNS (lines), LDA (symbols), and LST.

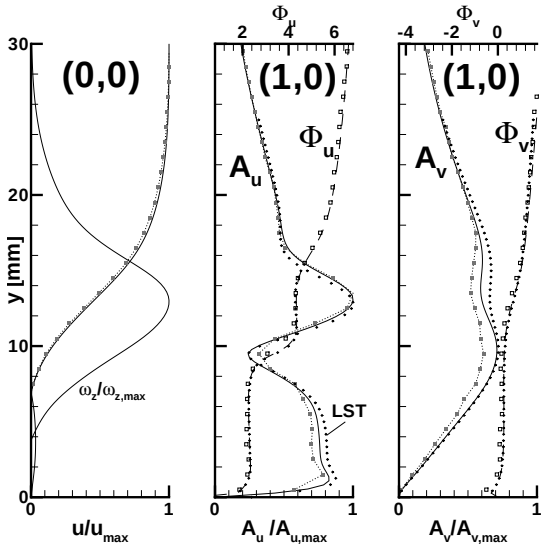

Fig. 7: TS amplitude and phase distributions. Results from DNS (lines), LDA (symbols), and LST at $x = 290\ mm$.

nature of the disturbance. Amplitude development predicted by LST is obtained by integrating the amplification rates of Fig. 5 in streamwise direction.

Wall-normal distributions of amplitudes and phases for the streamwise and wall-normal velocities are compared in Fig. 7 at a location around the middle of the region of linear amplification. The detached shear-layer corresponds to the part of maximum spanwise vorticity around $y = 12\ mm$. It is at this distance from the wall where the disturbance amplitude of the 2-D TS wave reaches maximum values for the u-velocity, as in the case of a Kelvin-Helmholtz instability.

5 Non-linear Disturbance Development

As can be seen from Fig. 6, calculation and experiment also predict the same amplitude, growth rate and saturation level for the non-linearly generated higher harmonic disturbance $(2, 0)$. Both disturbances saturate at the position of shear-layer roll-up (Fig. 8). At that streamwise position, strong vortical structures can be observed in a plane parallel to the wall (Fig. 9).

In the experiment, a strong initial steady disturbance with half the spacer wavelength $(0, 2)$ can be observed (Fig. 10). From the good agreement with LST for the development of the 2-D TS wave, as described in the previous section, it can be concluded that the spanwise modulation of the base flow does not exert

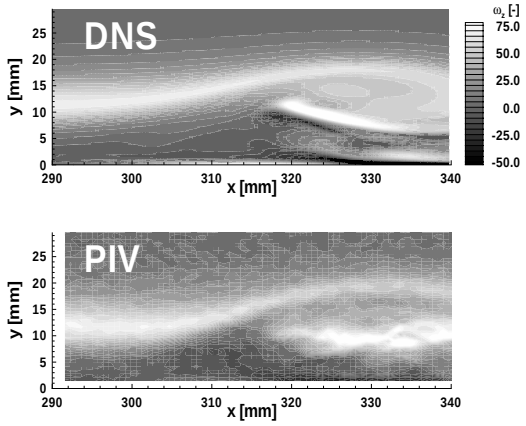

Fig. 8: Instantaneous view of spanwise vorticity ω_z at $z = 0\ mm$.

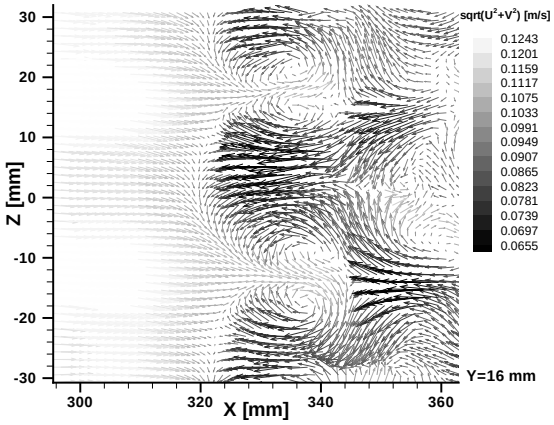

Fig. 9: Instantaneous view of wall-parallel velocities (PIV).

any influence on 2-D instability characteristics of the flow field. In contrast, the growth of spanwise modulated perturbations of fundamental frequency $(1, \pm 2)$ is decisively affected by the presence of this steady mode. Strong growth of these disturbances cannot be explained by linear theory (Fig. 5), nor by a secondary (convective [9] or temporal [6]) instability, since it already sets in well before the TS wave has gained a sufficiently large amplitude.

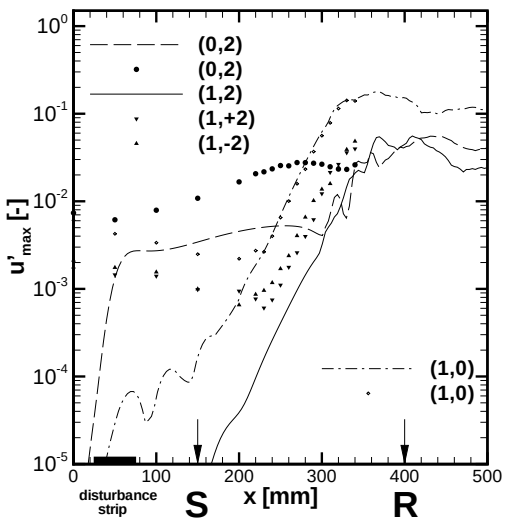

Fig. 10: Amplification of the max. velocity fluctuation u'_{max}. Results from DNS (lines) and LDA (symbols).

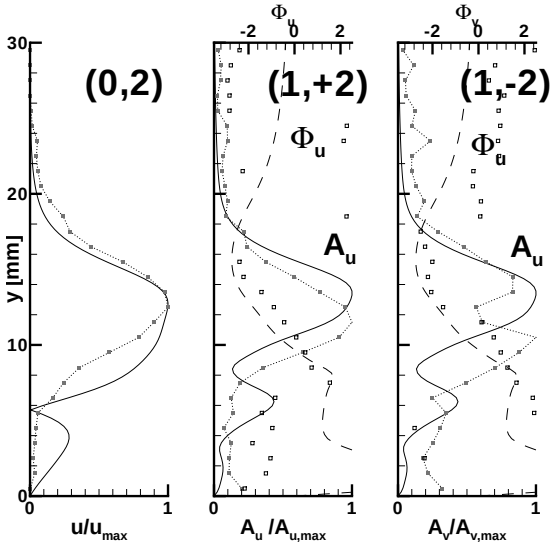

Fig. 11: Amplitude and phase distributions. Results from DNS (lines) and LDA (symbols) at $x = 290\ mm$.

Instead, non-linear interaction between the TS wave $(1, 0)$ and the large steady disturbance $(0, 2)$ generates modes $(1, \pm 2)$ with approximately the same ampli-

fication rate as mode $(1,0)$. Results from a spanwise-symmetrical DNS confirm this fact by showing the same growth rate for mode $(1,2)$ only in the presence of a large steady disturbance. Agreement of amplitude and phase distributions between experiment and DNS is reasonable (Fig. 11), albeit some deviations from symmetry can be seen in the measurements, which are not included in the DNS method in this study.

Despite the importance of three-dimensional disturbances for the breakdown to turbulence, the dominance of the two-dimensional fundamental perturbation even far downstream of reattachment is remarkable. Characteristics of the separation bubble have proven to be the same in a DNS with and without forced steady three-dimensional disturbances. The same holds for the experiment with and without spacers, suggesting that the large initial disturbance level plays only a minor role in the transition process. Instead, the dominating mechanism at work seems to be an absolute secondary instability of three-dimensional disturbances identified by Maucher et. al. [6] which is independent of the level of incoming 3-D disturbances. Differences in amplitude and amplification of DNS and experiment for mode $(0,2)$ are not critical.

6 Conclusions

A detailed comparison between measurements and numerical calculations of the velocity field in a transitional separation bubble showed very good agreement for time-averaged and the 2-D part of Fourier analyzed quantities. Transition in a separation bubble under consideration here is driven by convective primary amplification of 2-D TS waves, mainly determining the size and position of the bubble. This mechanism could be clearly identified from the existing numerical and experimental data. The formation of spanwise variations of the incoming 2-D flow field can be attributed to large steady perturbations and non-linearly generated time-dependent disturbances. The influence of the amplitude of these disturbances was found to be negligible.

References

[1] M. Alam and N. D. Sandham. Direct Numerical Simulation of 'Short' Laminar Separation Bubbles with Turbulent Reattachment. *J. Fluid Mech.*, 410:1–28, 2000.

[2] K. Augustin, U. Rist, and S. Wagner. Control of a Laminar Separation Bubble by Excitation of Boundary-Layer Disturbance Waves. In Wagner, Rist, Heinemann, and Hilbig, editors, *New Results in Numerical and Experimental Fluid Mechanics III.* 12^{th} Stab Symposium 2000, Stuttgart, NNFM 77 Springer-Verlag, Heidelberg, 2001.

[3] P.S. Klebanoff, K.D. Tidstrom, and L.M. Sargent. The Three-Dimensional Nature of Boundary-Layer Instability. *J. Fluid Mech.*, 12:1–41.

[4] M. Kruse and S. Wagner. LDA Measurements of Laminar-Turbulent Transition in a Flat-Plate Boundary layer. 8th International Symposium on Applications of Laser Techniques to Fluid Mechanics, 8.–11. July, Lisbon, Portugal, 1996.

[5] M. Lang, O. Marxen, U. Rist, S. Wagner, and W. Würz. LDA-Messungen zur Transition in einer laminaren Ablöseblase. In *Lasermethoden in der Strömungmesstechnik*. 8. Fachtagung der GALA, 12.–14. Sep. 2000, Freising-Weihenstephan, Shaker Verlag, Aachen, 2000.

[6] U. Maucher, U. Rist, and S. Wagner. Transitional Structures in a Laminar Separation Bubble. In W. Nitsche, H. Heinemann, and R. Hilbig, editors, *Notes on Numerical Fluid Mechanics*, volume 72, pages 307–314. Vieweg Verlag, Wiesbaden, 1999. 11^{th}Stab Symposium 98, Berlin.

[7] U. Maucher, U. Rist, and S. Wagner. Refined Interaction Method for Direct Numerical Simulation of Transition in Separation Bubbles. *AIAA Journal.*, 38(8):1385–1393, 2000.

[8] U. Rist. Nonlinear Effects of 2D and 3D Disturbances on Laminar Separation Bubbles. Proceedings of IUTAM Symposium on Nonlinear Instability of Nonparallel flows.

[9] U. Rist. Zur Instabilität und Transition in laminaren Ablöseblasen. Habilitation, Universität Stuttgart, Shaker Verlag, Aachen, 1998.

[10] P.R. Spalart and M. Kh. Strelets. Mechanisms of Transition and Heat Transfer in a Separation Bubbles with Turbulent Reattachment. *J. Fluid Mech.*, 403:329–349, 2000.

[11] M. Strunz and J. F. Speth. A New Laminar Water Tunnel to Study the Transition Process in a Blasius Boundary Layer and in a Separation Bubble and a New Tool for Industrial Aerodynamics and Hydrodynamic Research. *AGARD CP-413*, pages 25–1–25–5, 1987.

[12] J.H. Watmuff. Evolution of a Wave Packet into Vortex Loops in a Laminar Separation Bubble. *J. Fluid Mech.*, 397:119–169, 1999.

[13] Z. Yang and P. R. Voke. Large-Eddy Simulation of Boundary-layer and Transition at a Change of Surface Curvature. *J. Fluid Mech.*, 439:305–333, 2001.